The roles of 3′-exoribonucleases and the exosome in trypanosome mRNA degradation

ABEER FADDA,[1] VALENTIN FÄRBER,[1] DOROTHEA DROLL, and CHRISTINE CLAYTON[2]
Zentrum für Molekulare Biologie der Universität Heidelberg, DKFZ-ZMBH Alliance, D69120 Heidelberg, Germany

ABSTRACT

The degradation of eukaryotic mRNAs can be initiated by deadenylation, decapping, or endonuclease cleavage. This is followed by 5′–3′ degradation by homologs of Xrn1, and/or 3′–5′ degradation by the exosome. We previously reported that, in African trypanosome *Trypanosoma brucei*, most mRNAs are deadenylated prior to degradation, and that depletion of the major 5′–3′ exoribonuclease XRNA preferentially stabilizes unstable mRNAs. We now show that depletion of either CAF1 or CNOT10, two components of the principal deadenylation complex, strongly inhibits degradation of most mRNAs. RNAi targeting another deadenylase, PAN2, or RRP45, a core component of the exosome, preferentially stabilized mRNAs with intermediate half-lives. RRP45 depletion resulted in a 5′ bias of mRNA sequences, suggesting action by a distributive 3′–5′ exoribonuclease. Results suggested that the exosome is involved in the processing of trypanosome snoRNAs. There was no correlation between effects on half-lives and on mRNA abundance.

Keywords: mRNA degradation; mRNA decay; exosome; deadenylation; CAF1; PAN2; *Trypanosoma*

INTRODUCTION

The abundance of an mRNA in a cell is determined not only by its rate of synthesis and processing, but also by its decay rate. There are three ways in which degradation of an mRNA can begin: by removal of the 3′ poly(A) tail or the 5′ cap structure (Li and Kiledjian 2010), or by endonucleolytic digestion (Schoenberg 2011). For most eukaryotic mRNAs that have been studied, constitutive degradation is initiated by deadenylation (Chen and Shyu 2011). Three different types of cytosolic deadenylase are known. Poly(A) ribonuclease (PARN) is involved mainly in specialized processes (Chen and Shyu 2011); PAN2 deadenylase, in a complex with PAN3, has a minor role, perhaps in initial shortening of poly(A) tails (Yamashita et al. 2005). The major activity resides in the Ccr4/Caf1/Not complex (Collart and Panasenko 2012), which consists of the central scaffold protein Not1, Not2, Not3 and/or Not5, Caf40, either Caf130 or CNOT10, the exoribonuclease Caf1, and, in Opisthokonts, an additional exoribonuclease, Ccr4 (Collart and Panasenko 2012). Shortening of the poly(A) tail to <20 nt leads to loss of poly(A) binding protein, which is followed by decapping. Some mRNAs are subjected to deadenylation-independent decapping, or to specific endonuclease cleavage. In each case, the mRNA is then exposed to 5′–3 degradation by the Xrn1 exonuclease, or 3′–5′ degradation by the exosome (Chen and Shyu 2011).

Models of eukaryotic mRNA decay were established using a very small selection of specific transcript sequences but have been followed by transcriptome-wide analyses. Deletions of Ccr4 and Pan2 in yeast caused stabilization of mRNAs encoding ribosomal proteins and ribosome biogenesis factors (Grigull et al. 2004): These mRNAs are among the least stable in yeast. More recently, *Saccharomyces cerevisiae* mRNA decay rates were measured by 4-thio-uracil pulse-chase labeling, and a median half-life of 11–12 min was measured (Miller et al. 2011). Interestingly, cells expressing a mutant RNA polymerase II with slow elongation compensated by decreasing mRNA degradation; conversely, cells lacking Ccr4p or Caf1p had globally decreased mRNA degradation and compensated via decreased mRNA synthesis (Sun et al. 2012). In the latter case, deletion of *CAF1* had the stronger effect, since it abolishes deadenylation by the Not complex: The average half-life increased over sixfold, while synthesis decreased 2.6-fold (Sun et al. 2012).

The exosome core has nine subunits: a central hexamer surmounted by three S1-domain proteins. Exosome core components are essential, since the exosome is required for processing of many stable RNAs including rRNA, in addition to mRNA. Exosome RNase activity is contributed by associated 3′–5′ exoribonucleases: Rrp6p (mainly restricted to the nucleus in mammals and yeast) and Rrp44p (mainly in the cytoplasm). Shutting off expression of a core exosome component in yeast caused increases in mRNAs for ribosome

[1]These authors contributed equally to this work.
[2]**Corresponding author**
E-mail cclayton@zmbh.uni-heidelberg.de
Article published online ahead of print. Article and publication date are at http://www.rnajournal.org/cgi/doi/10.1261/rna.038430.113.

biogenesis, processing of 20S RNA, and nucleo-cytoplasmic transport (Mnaimneh et al. 2004). Reduction of a different core component, however, resulted in a decrease in mRNAs encoding ribosomal components, which was attributed to growth arrest (Houalla et al. 2006). Depletion of an exosome subunit in *Drosophila* cells caused increases in steady-state levels of ~1000 different mRNAs (Kiss and Andrulis 2010); mRNAs involved in the cell cycle and development were preferentially affected, as were mRNAs with unusually long untranslated regions. Only 60 mRNAs were decreased. Inducible RNAi against *Arabidopsis* exosome subunits revealed increases in ~250 specific mRNAs, as well as various novel RNAs, and RNAs with unexpected 3′ extensions (Chekanova et al. 2007). The exosome is involved in the processing of snRNAs and snoRNAs; the absence of Rrp6p or other exosome subunits results in an accumulation of precursors, including polyadenylated degradation intermediates, in both yeast (Wyers et al. 2005; Gudipati et al. 2012) and *Arabidopis* (Chekanova et al. 2007). Increases in mRNAs located downstream from snoRNA loci were also observed (Houalla et al. 2006).

The transcription of protein-coding genes in Kinetoplastid protists by RNA polymerase II is polycistronic (Palenchar and Bellofatto 2006; Daniels et al. 2010). Individual mRNAs are excised by 5′ *trans* splicing of a "spliced leader" (*SL*) and 3′ polyadenylation (Michaeli 2011). Since transcription of individual genes cannot be controlled, mRNA turnover plays an unusually dominant role in determining mRNA abundance (Ouellette and Papadopoulou 2009; Fernández-Moya and Estévez 2010; Kramer and Carrington 2011; Manful et al. 2011). For most mRNAs, removal of the poly(A) tail precedes degradation of the remainder of the transcript (Manful et al. 2011). A typical mRNA degradation machinery is present: an exosome (Estévez et al. 2001, 2003); a scavenger decapping enzyme (Banerjee et al. 2009); an Xrn1 homolog, XRNA (Li et al. 2006); PAN2/PAN3 (Schwede et al. 2009); PARN (Milone et al. 2004; Utter et al. 2011); a CAF1/NOT complex composed of CAF1, CAF40, NOT1, NOT2, NOT3/5 (Schwede et al. 2008); a CNOT11 homolog (Schwede et al. 2008; Mauxion et al. 2013); and CNOT10 (Färber et al. 2013). Only a Dcp2-like decapping enzyme is missing (Schwede et al. 2009). RRP45 is an essential structural component of the exosome; its depletion results in complex disassembly and instability of other exosome subunits (Estévez et al. 2001, 2003). Similarly, CNOT10 is required for the attachment of the deadenylase CAF1 to the CAF1/NOT complex (Färber et al. 2013).

The median mRNA half-life in bloodstream-form trypanosomes (the form that grows in mammals) is ~15–20 min (Manful et al. 2011). Depletion of XRNA (Li et al. 2006), PAN2 (Schwede et al. 2009), or the exosome (Haile et al. 2003) delayed the degradation of the highly unstable developmentally regulated mRNA encoding EP procyclin, or reporter mRNAs bearing its 3′ UTR; *ACT* (actinA) mRNA, which has a half-life at the median, was also stabilized by RNAi targeting *PAN2*, and the developmentally regulated unstable mRNA encoding pyruvate phosphate decarboxylase was stabilized by *RRP45* RNAi. In contrast, depletion of CAF1 (Schwede et al. 2008, 2009) or CNOT10 (Färber et al. 2013) affected all mRNAs examined. Detailed studies of *EP* mRNA degradation kinetics provided clear evidence for a very rapid, deadenylation-independent, and XRNA-dependent 5′–3′ pathway, combined with a slower deadenylation-dependent component (Irmer and Clayton 2001; Haile et al. 2008; Schwede et al. 2009). In the related Kinetoplastid parasite *Leishmania* there is also evidence for this type of biphasic degradation (Haile et al. 2008), and some developmentally unstable mRNAs are subject to endonuclease cleavage in the 3′ UTR (Muller et al. 2010). So far, endonucleolytic pathways have not been found in trypanosomes.

Transcriptome-wide analysis of trypanosome mRNA half-lives in cells after *XRNA* RNAi demonstrated that XRNA depletion inhibited the degradation of unstable mRNAs, while some of the more stable mRNAs had shorter half-lives (Manful et al. 2011). We have now extended this to all the known factors involved in degradation from the 3′ end: PAN2, the exosome, and components of the CAF1/NOT complex. Our results confirm that the CAF1/NOT complex is central to RNA turnover in trypanosomes, while depletion of the exosome and PAN2 complexes mainly delayed degradation of mRNAs with median half-lives.

RESULTS

The rate of bulk mRNA degradation in wild-type cells

The aim of this work was to assess the transcriptome-wide role of 3′ pathways in mRNA degradation, using RNA-seq. We first, however, show results for bulk mRNA. Given the unusual mode of trypanosome mRNA synthesis and processing, to inhibit creation of new mRNAs, we need to inhibit not only transcription, but also processing of preexisting precursors. To inhibit processing, we therefore first added Sinefungin, which inhibits methylation of the 5′ cap of the *SLRNA* used as a donor for the 5′ 39-nt spliced leader (*SL*). Unmethylated *SLRNA* is not a substrate for *trans* splicing (Ullu and Tschudi 1991). Five minutes later, when we expected reduced cap methylation, we added Actinomycin D (Colasante et al. 2007).

Since all trypanosome mRNAs carry the *SL* at the 5′ end, the abundance of the *SL* can serve as a proxy for the abundance of total mRNA, independently of the presence of a poly(A) tail. To determine the average half-life of the bulk mRNA population, we therefore hybridized Northern blots with an *SL* probe. As previously shown (De Lange et al. 1984), a smear was obtained, with more prominent areas at the positions of abundant mRNAs. Figure 1 shows results for samples that were later subjected to RNA-seq, while Supplemental Figure S1 shows more detailed time courses. The *SLRNA* (arrow, Fig. 1) is the 5′ substrate for *trans* splicing, which consists of the 5′ *SL* and the *SL* intron. The *SLRNA* disappeared rapidly after

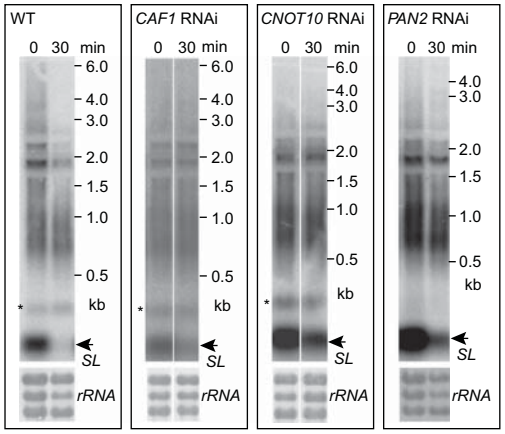

FIGURE 1. Spliced leader hybridization to Northern blots of the RNA samples sent for sequencing. RNA from different cells was prepared and subjected to Northern blotting with a spliced leader RNA 39mer oligonucleotide probe. Three similar samples were tested for each line; one typical lane is shown. A second set of lanes from wild-type (WT) and *CNOT10* RNAi was shown in Färber et al. (2013). The arrow points to the spliced leader precursor RNA, and the asterisk marks signal from the 7SL (signal recognition particle) RNA left from a previous hybridization. The mRNA signal was quantitated in the region from ~400 nt to 6 kb. The panel *below* shows the methylene blue signal from rRNA on the corresponding blot segments. The hybridization signals for individual RNAi lines differ because RNA from each cell line was run on a different gel. For further comparisons see Supplemental Figure S1.

Actinomycin D addition to wild-type cells; *SLRNA* with methylated caps could be used in splicing, while the remainder was presumably degraded (Fig. 1; Supplemental Fig. S1). To assess mRNA levels, the density of the smear >400 nt was measured, then relative amounts were calculated using rRNA or the *7SL* (signal recognition particle RNA) as a standard. The results for RNA preparations that were subsequently used for RNA-seq (Fig. 1) are listed in Table 1. The proportion of *SL* signal that remained after 30-min transcription inhibition in wild-type cells was 50%–60% (Table 1), which was approximately in agreement with our previous estimates based on the abundances of individual mRNAs (Haanstra et al. 2008; Manful et al. 2011).

Supplemental Figure S1A shows the time course of disappearance of *SL* signal over a 2-h time course. Three independent experiments yielded half-lives between 44 and 46 min, with 54%–56% of *SL* signal remaining after 30 min (Supplemental Fig. S2).

The rate of bulk mRNA degradation in cell lines deficient in 3′–5′ RNA degradation pathways

To analyze the roles of deadenylation and the exosome in global mRNA decay, we used cell lines in which the mRNAs encoding CAF1 (Tb927.6.600), CNOT10 (Tb927.10.8720), PAN2 (Tb927.6.1670), or RRP45 (Tb927.6.670, an essential core component of the exosome) were depleted. For the RNA-seq analyses, we used existing cell lines (Estévez et al. 2001; Schwede et al. 2008, 2009; Färber et al. 2013). All lines were checked for the effectiveness of RNAi, by Northern blotting and by ensuring that growth was inhibited within 48 h of RNAi induction (data not shown), and later, more accurately, by analysis of the RNA-seq results (Table 1). For all experiments, RNAi was induced for 24 h; this time point precedes the onset of growth inhibition. Analysis of the amounts of *SL*-bearing mRNA that remained after 30-min Actinomycin D indicated that the bulk mRNA decay rates in cells with *PAN2* RNAi differed little from wild type, whereas for *CAF1*, mRNA degradation was almost completely inhibited (Fig. 1; Table 1). The strong inhibition of mRNA decay after *CNOT10* RNAi was previously reported (Färber et al. 2013) and is illustrated again in Table 1, Figure 1, and Supplemental Figure S1. Bulk mRNA degradation in *RRP45* RNAi lines is discussed in the next section.

Results for 2-h time courses of *SL*-mRNA degradation are shown in Supplemental Figure S1 and quantitation is in Supplemental Figure S2. These experiments were done later than those in Figure 1. In part, new cell lines had to be made

TABLE 1. Characteristics of mRNA degradation in exoribonuclease mutants

Cell line	WT	RRP45	PAN2	CAF1	CNOT10	XRNA
Average fold target mRNA decrease[a]	—	3×	11×	2×	82×	
SL mRNA at 30 min[b]	55 ± 22%	ND	60 ± 2%	93 ± 19%	102 ± 14%	
TUB mRNA at 30 min[b]		76 ± 5%	ND	~100%	~100%	
HISH4 mRNA at 30 min[b]		66 ± 6%	ND	~100%	~100%	
No. of mRNAs with half-life >120 min[a]	146	199	506	1616	4471	16
Median bulk mRNA half-life (min)[a]	12	14	15	32	>240	18
Arithmetic mean bulk mRNA half-life (min)[a]	21	25	39	90	>200	21

Results for wild-type and XRNA-depleted cells are from Manful et al. (2011).
[a]Results from RNA-seq; for the calculations only the 5326 "unique genes" of Siegel et al. (2010), and only ORFs with an RPM of at least 5 at steady state were included.
[b]These are the results for 0- and 30-min time points, measured by Northern blotting, for the samples that were prepared for sequencing. The *SLRNA* signals were normalized to the *7SL* RNA signal but were also checked using the methylene blue rRNA stain. If a standard deviation is shown, the data are for three samples prepared for RNA-seq, of which two were actually sequenced; If no standard deviation is shown (CAF1 and CNOT10, *TUB* and *HISH4*), only two samples are included. No results are shown for XRNA since the data used for comparisons are from an earlier paper (Manful et al. 2011).

because the effectiveness of the RNAi in the stored cell lines had diminished. This means that the results for RNA-seq (Fig. 1; Table 1) and for the 2-h time courses can be compared only qualitatively. In the 2-h experimental series, RNAi targeting *XRNA*, *PAN2*, and *RRP45* had no consistent effect on bulk mRNA turnover (Supplemental Figs. S1B–D, S2), whereas, once again, depletion of either CAF1 or CNOT10 strongly delayed mRNA degradation (Supplemental Figs. S1E,F, S2). RNAi targeting *CAF1* was, in these experiments, somewhat more effective than RNAi targeting *CNOT10* in inhibition of mRNA decay; this can be attributed to the use of new cell lines with different RNAi penetrance.

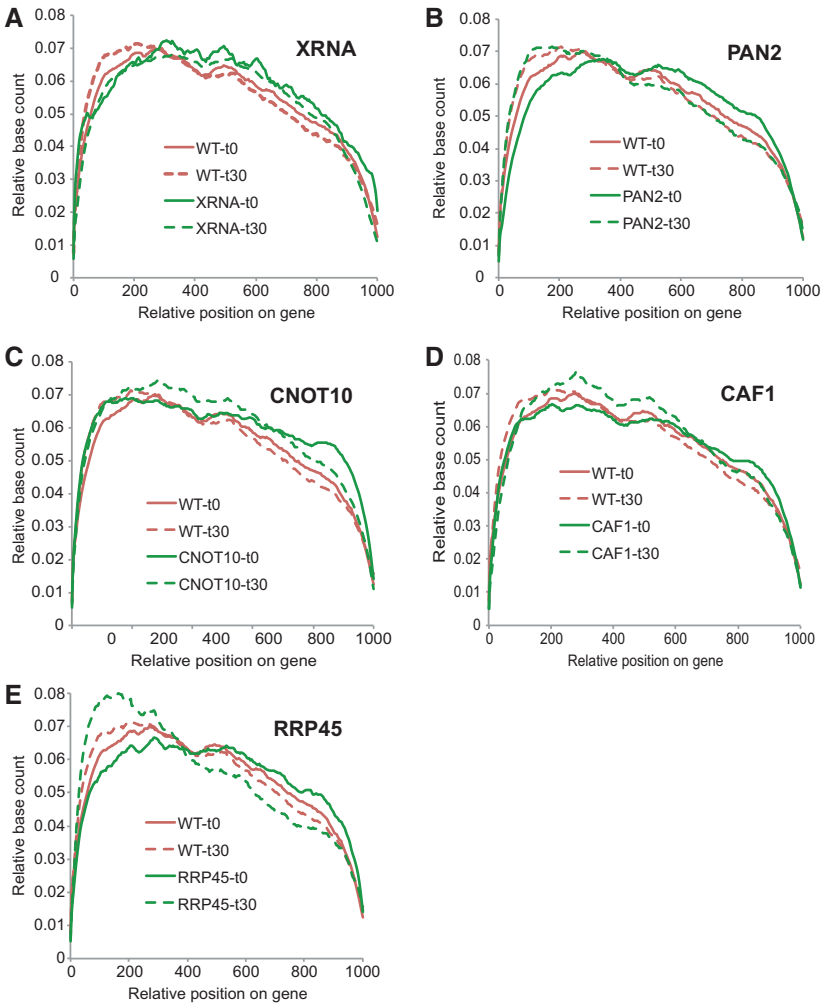

FIGURE 2. Depletion of *RRP45* results in a 5′ read bias. Predominant polyadenylation and splice acceptor sites for as many mRNAs as possible were extracted from all our data sets. For each unique ORF, the read density was plotted across the entire predicted mRNA, then normalized to an mRNA length of 1000 nt. The average read density across all mRNAs was then plotted. Results for RNAi lines are compared with wild type, as indicated on the individual panels (*A–E*).

Depletion of RRP45 results in a 5′ read bias

We used RNA-seq to examine transcriptomes at steady state and 30 min after inhibition of mRNA maturation and synthesis with Sinefungin and Actinomycin D, respectively. From the three replicates used to estimate the disappearance of the *SL* signal (Table 1), two were sent for sequencing. All raw data (read counts) are in Supplemental Table 1 and the numbers of aligned reads are shown in Supplemental Figure S3. We intended to use the *SL* hybridization signal (examples in Fig. 1) to normalize our RNA-seq data, but this is only valid if the 5′ end is representative of the whole mRNA. We therefore examined the distributions of read counts across the mRNAs both before and after addition of inhibitors. For this purpose, we extracted the most commonly used 5′ splice and 3′ polyadenylation sites from our data. Next, for every mRNA that had mapped extremities, we normalized the read density results to a standardized length of 1 kb. This enabled us to plot the average read densities for all mRNAs irrespective of length. Results are shown in Figure 2. For untreated cells there was a mild decrease in density toward the 3′ end (Fig. 2). Sometimes, this decrease already started within the mRNA coding region (data not shown). In the wild-type cells, after 30-min transcription inhibition, the read density pattern had hardly changed; the mRNA population at 30 min therefore presumably consisted mainly of intact mRNAs (Fig. 2).

Next, we compared the distributions for the RNAi cell lines, incorporating also our previous results from *XRNA* RNAi (Manful et al. 2011). The overall distributions, both at steady state and after 30-min Actinomycin D, were in general similar to wild type (Fig. 2A–D). However, for cells with *RRP45* RNAi after 30-min Actinomycin D, there was a clear read bias toward the 5′ end (Fig. 2E). This suggests that the cells contained mRNAs that were in various stages of 3′–5′ degradation. For these cells, therefore, we could not use *SL* signals in order to normalize the data, and relied on α tubulin instead (see below).

Inhibition of 3′–5′ pathways preferentially affects more stable mRNAs

We next used the transcriptome data to obtain estimates of mRNA half-lives for all ORFs, assuming simple exponential decay (Supplemental Table S2). Since the *SL* results were probably biased in the RRP45 samples, we normalized those based on degradation of the α tubulin mRNA (Table 1), which was very similar to wild type (data not shown). The remainder

were normalized using the *SL* Northern blot measurements from the original RNAs and additional replicates that were made at the same time (Fig. 1; Table 1). We selected all unique ORFs, and added up the total read counts obtained from them. From these, we calculated reads per million (RPM) for all ORFs. For example, for PAN2, in which 60% of total mRNA remains after 30 min (Table 1), all RPMs from the 30-min time points were multiplied by 0.6. The 30-min RPM for CAF1 and CNOT10 were not changed since no significant degradation of total mRNA had occurred after 30 min. Results for the duplicates were reproducible (log scale correlation coefficients exceeding 0.85), with most variation being concentrated at low read densities (Supplemental Fig. S3). For most subsequent calculations, we therefore considered only mRNAs represented by at least 5 RPM at time 0 in the wild-type sample. The use of a single time point gives only a very crude estimate of the half-life: Complex kinetics (Deneke et al. 2013) are not detected, and since we are extrapolating, the more the half-life differs from 30 min, the greater the error is likely to be. For the figures and tables the maximum half-life was arbitrarily set to 240 min.

Despite the limitations of our approach, some conclusions can be drawn. The clearest result was that depletion of *PAN2* (Fig. 3A) or *RRP45* (Fig. 3B) had much less effect on the half-life distribution than depletion of *CAF1* (Fig. 3C) or *CNOT10* (Fig. 3D). Impairing CAF1/NOT complex function

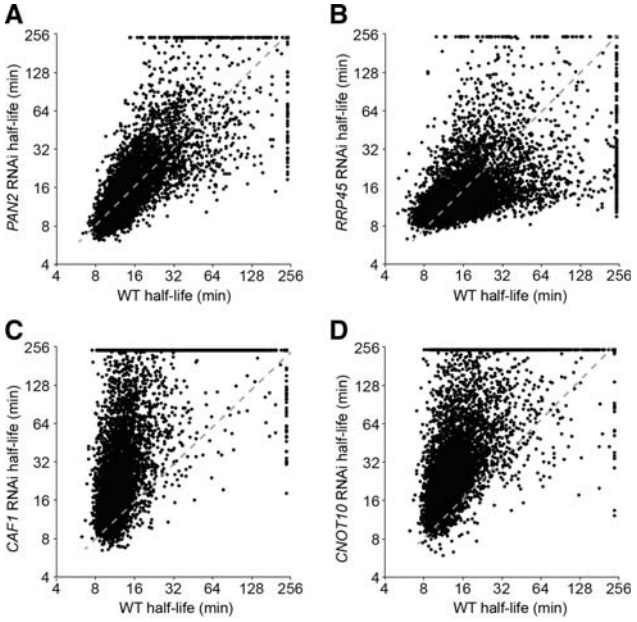

FIGURE 3. Effect of RNAi on the half-lives of trypanosome mRNAs. The half-life of the mRNA from each unique ORF in cells with RNAi is plotted against the half-life that was previously measured for wild-type cells, on a log scale. The dashed diagonal indicates perfect correlation. All half-lives >240 min were set to 240 min, and all ORFs with a steady-state RPM of <5 for any of the cell lines were excluded from the data set. RNAi was as follows: (*A*) *PAN2*; (*B*) *RRP45*; (*C*) *CAF1*; (*D*) *CNOT10*.

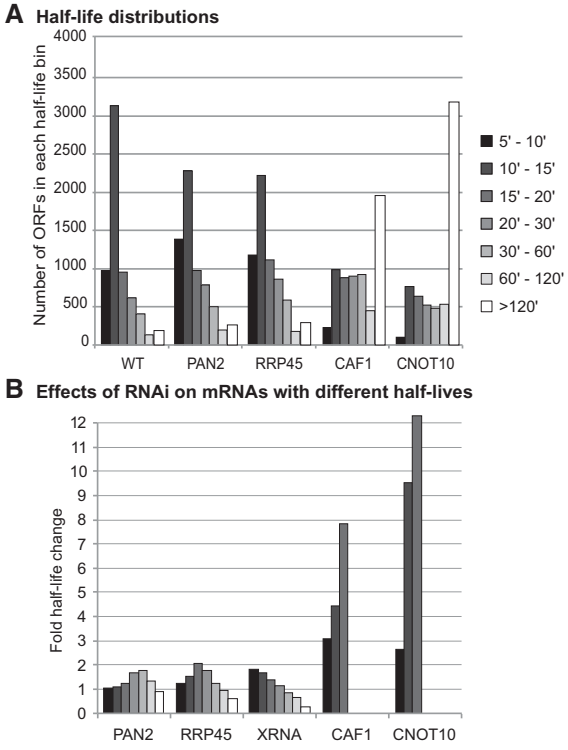

FIGURE 4. Effect of RRP45, PAN2, and CAF1/NOT complex depletion on mRNA decay. (*A*) Effects on the overall half-life distribution. Each unique ORF was placed in a half-life category as indicated in the key on the *right*. The numbers of ORFs in each category are displayed. (*B*) The half-life for each unique ORF after RNAi was divided by the half-life in wild type. The ORFs were then organized into categories depending on the wild-type half-life, and the average change in half-life after RNAi was calculated. The differences between the means of the categories for all RNAi lines were significant (one-way ANOVA on linearized data *P*-value $<1 \times 10^{-16}$).

delayed degradation of almost all mRNAs, with most now having half-lives >60 min. Thus it was clear that, for the vast majority of mRNAs, deadenylation by the CAF1/NOT complex is a critical event in the onset of mRNA decay. CNOT10 is required for attachment of CAF1 to the remaining NOT subunits and for CAF1 deadenylation activity in vivo (Färber et al. 2013). *CNOT10* RNAi had a stronger effect on mRNA decay than *CAF1* RNAi, but *CNOT10* RNA was also more effectively depleted (>10× reduction as opposed to only 2× for CAF1). Moreover, CAF1 protein is present in excess (Färber et al. 2013). In subsequent discussions, we will therefore treat the two sets of results together, assuming that the difference between the two is only due to variations in the effectiveness of the RNAi.

We next looked at the distributions of half-lives. To do this, each unique ORF was placed into a half-life category, then the number of ORFs in each category was counted (Fig. 4A). In wild-type cells, we had previously found that most mRNAs had half-lives <20 min, with very few >1 h (Fig. 4A; Manful et al. 2011). Depletion of PAN2 and RRP45 had little effect on the overall distribution, whereas disabling the CAF1/NOT

complex shifted many mRNAs into the longer-lived categories (Fig. 4A). To see whether mRNAs with particular characteristics were specifically affected by inhibition of different 3′–5′ degradation pathways, we first calculated for each ORF the ratio between the wild-type half-life and the new half-life. We then grouped mRNAs according to their half-lives in wild-type cells, and plotted the average ratio for each group. Note that, because of our arbitrary maximum half-life of 240 min, an mRNA with a wild-type half-life of 120 min cannot increase more than twofold in the tables, so effects on more stable mRNAs may be underestimated. We had previously found that, after XRNA depletion, mRNAs with short half-lives were specifically stabilized, whereas mRNAs with longer half-lives were destabilized (Manful et al. 2011); this is again illustrated in Figure 4B. The effects of PAN2 and RRP45 depletion were different: mRNAs with intermediate half-lives were stabilized, but again, for RRP45, the long-half-life mRNAs appeared to be less stable (Fig. 4B). CAF1 and CNOT10 depletion also affected the least stable mRNAs less than those of intermediate stability. The significance of these different effects for all cell lines was confirmed by one-way ANOVA. Since many mRNAs with wild-type half-lives >20 min had no measurable degradation in these two mutants, no data for these are plotted because the fold effect could not be calculated.

Changes in mRNA decay are not reflected in steady-state abundance

We next examined the effects of RNAi on the steady-state abundances of mRNAs. There was no effect on bulk mRNA abundance, as judged by the *SL* signal (Supplemental Fig. 1G). We had previously seen that, after XRNA depletion, unstable mRNAs became slightly more abundant than in wild-type (Manful et al. 2011), although the correlation was very weak. The drastic inhibition of mRNA decay seen after inhibition of the CAF1/NOT complex would be expected to have far greater effects. When, however, we examined the abundances of mRNAs after RNAi against CNOT10, RRP45, or PAN2 there was no correlation at all between the changes in half-life and those in mRNA abundance (Fig. 5; Table 2; Supplemental Table S3). For RRP45 and PAN2 knockdowns, there were many ORFs showing altered mRNA abundance despite little change in half-life. To examine this further, for the CAF1/NOT complex, we looked at mRNAs that had half-lives of <240 min in both wild-type and *CAF1* RNAi cells. The presence of a significant expression change for an ORF (*P*-adjusted-value <0.01) was not predictive of an alteration in mRNA decay rate.

To check whether the discrepancy between change in abundance and change in half-life was in any way dependent on the position of genes in a transcription unit, we divided the change in abundance by the change in half-life for each unique gene. We then, for chromosomes 1, 2, and 3, plotted the results in the correct gene order. The distribution of effects appeared to be random, both between transcription units and with respect to position of a gene relative to the transcription start site.

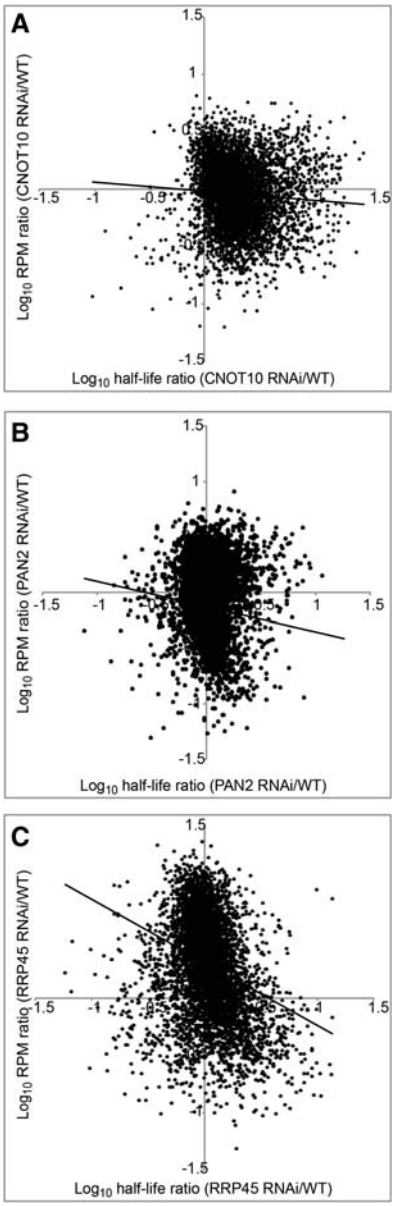

FIGURE 5. Changes in mRNA half-lives after RNAi do not lead to corresponding changes in mRNA abundance. The mRNA half-life after RNAi (in minutes) was divided by that in wild-type cells and plotted on the *x*-axis ($\log_{10}$); the mRNA abundance after RNAi (average RPM reads) was divided by that in wild-type cells and plotted on the *y*-axis ($\log_{10}$). mRNAs with half-lives >240 min were excluded. Trend lines were plotted in Excel. (*A*) *CNOT10* RNAi; (*B*) *PAN2* RNAi; (*C*) *RRP45* RNAi.

RNAi targeting 3′–5′ decay preferentially affects mRNAs encoding proteins with specific functional classes

We next looked to see whether the steady-state levels, or half-lives, of mRNAs encoding particular functional classes of proteins were differentially affected by inhibition of 3′–5′ mRNA

TABLE 2. Statistics for genes showing changed expression at steady state

	Number of differentially expressed genes		Mean fold change in half-life, for genes with mRNA that was:		Mean WT half-life (min) for genes with mRNA that was:	
RNAi target	increased	decreased	increased	decreased	increased	decreased
CNOT10	96[a]	305[a]	6.0	3.2	45	55
CAF1	714	708	3.0	9.0	32	30
PAN2	439	761	1.5	1.3	34	24
RRP45	1049	1224	1.0	2.8	25	30

We included only unique genes (according to Siegel et al. [2010] with a few manual additions), with a minimum of 5 RPM at steady state and 1 RPM after 30-min Actinomycin D. The mRNA abundance was judged to be increased or decreased when it was statistically significant.
[a]The low number of differentially expressed genes for CNOT10 is a technical artifact, as for many genes the difference between replicates was too big to allow a clear statement to be made.

decay. To classify trypanosome genes, we supplemented the current annotations from GeneDB and TritrypDB with KEGG designations and a limited number of publications describing pathways and organellar or complex proteomes (Supplemental Table S2; Bringaud et al. 2006; Colasante et al. 2006; Michels et al. 2006; Panigrahi et al. 2008; Vertommena et al. 2008; Acestor et al. 2009; Droll et al. 2013). We had already seen that, in wild-type cells, mRNAs encoding ribosomal proteins and enzymes of glucose metabolism are significantly more stable than the average (Manful et al. 2011).

First we examined steady-state mRNA levels. In all of the mutants, ribosome-related genes (mostly encoding ribosomal proteins) were significantly enriched in the group of mRNAs that were significantly increased in abundance (Fisher test *P*-value $<1 \times 10^{-8}$) (Supplemental Table S3). In contrast, cytoskeleton-related genes were significantly enriched in the group showing significantly decreased mRNA abundance (Fisher test *P*-value $<1 \times 10^{-8}$) (Supplemental Table S3).

We now looked for functional classes that were enriched in the group of mRNAs that had an increase of at least twofold in their half-life (Fig. 6). For both *RRP45* and *PAN2* RNAi, mRNAs encoding cytoskeletal proteins were very significantly enriched in the stabilized category, and those encoding chaperones were stabilized by *PAN2* RNAi. The most notably destabilized categories were mRNAs encoding enzymes of glucose and glycerol metabolism, and RNA-binding proteins (Fig. 6). Developmentally regulated mRNAs were not specifically stabilized by depletion of any of the 3′–5′ decay pathway components (data not shown). No general enrichment analysis was done for the NOT complex mutants since the majority of mRNAs were stabilized.

RNAi targeting RRP45 results in increased read counts from snoRNA precursors

Many trypanosome snoRNAs are processed from longer precursors (Doniger et al. 2010; Michaeli et al. 2012). The snoRNAs themselves are much too small to be reliably retained in our data set, but precursors of >250 nt could have been detected. It was therefore interesting that there were far more snoRNA reads from the *RRP45* RNAi cells than from either wild type or any of the other mutants (Supplemental Table S3; Supplemental Figs. S4, S5). Examination of the raw data (Supplemental Figs. S4, S5) confirmed that RNA sequence reads from snoRNA clusters were spread across both the mature snoRNA and the neighboring regions. This strongly suggests that the exosome is involved in snoRNA processing in trypanosomes, as was previously demonstrated in other species (see Introduction).

DISCUSSION

We have shown here that a reduction in CAF1/NOT complex activity, effected through depletion of mRNA encoding either the CNOT10 or CAF1 subunit, inhibits the degradation of most trypanosome mRNAs. Depletion of either RRP45 or PAN2 affected much smaller subsets of mRNAs, which mostly did not overlap with each other (Fig. 7). Changes in mRNA half-life did not generally correlate with alterations in mRNA abundance, showing that additional regulatory mechanisms must be present.

In yeast with mutations in mRNA degradation, changes in mRNA decay were not reflected in mRNA steady-state abundance (Sun et al. 2012), and the suggested explanation was that feedback controls on transcription compensate for the lack of mRNA decay. The lack of correlation in trypanosomes is much more difficult to understand, because trypanosomes cannot alter the transcription rates of individual genes. Transcription by RNA polymerase II was clearly still active at the time we did our experiments; otherwise, a 30-min incubation with Actinomycin D would have had no effect at all on the relative abundances of different mRNAs and no mRNAs would have appeared to retain short half-lives. The most obvious possibility is that changes in *trans* splicing compensate for defects in mRNA degradation.

RNAi targeting PAN2 and RRP45 accelerated the degradation of quite a large number of mRNAs. These were enriched in categories that are required for growth, such as ATP generation from glucose and glycerol, vesicular transport, nucleotide metabolism, and translation. One possibility is that the effects were secondary to the onset of growth inhibition. It was notable that RNA-binding proteins were also particularly enriched in the destabilized category; perhaps some changes in mRNA stability or abundance reflected loss of regulatory RNA-binding proteins.

The read densities at steady state were not uniform across the whole length of mRNAs. Instead, densities were roughly

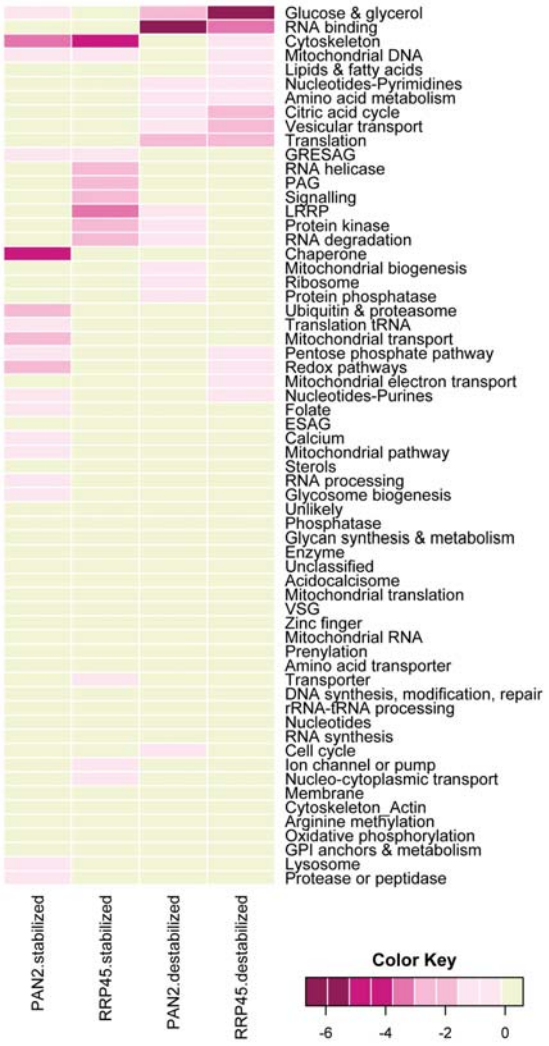

FIGURE 6. The effects of RNAi against *PAN2* and *RRP45* on genes encoding proteins of different functional classes. All unique ORFs were assigned into categories according to the function of the encoded protein. Those with mRNA stabilization or destabilization of at least twofold were selected, and the relative enrichment of each functional class was then calculated. Rows represent gene classes; columns represent the stabilized or destabilized mRNA. Each rectangle is colored to represent the log *P*-values for the enrichment of the corresponding functional category, according to Fisher's test. The darker the pink color, the more significant the enrichment (see key).

uniform across the first 2/3, then gradually declined toward the 3′ end. This could be a technical artifact. Both gene length and nucleotide composition can affect the patterns of RNA fragmentation and fragment amplification, resulting in clear biases in RNA-seq results (see for example Dohm et al. 2008; Sendler et al. 2011; Zheng et al. 2011). We have, however, found no base bias in our results (Manful et al. 2011). Another contributing factor could be the fact that possible polyadenylation sites in trypanosome mRNAs can be distributed over large distances—in extreme cases, several kilobases (Kolev et al. 2010; Nilsson et al. 2010; Siegel et al. 2010). The most frequently used poly(A) site will often be downstream from several other, less frequently used sites, so that the steady-state mRNA population is certain to contain some mRNAs with shorter 3′ UTRs.

After RNAi targeting PAN2, CAF1, or CNOT10, the distributions of sequence reads across RNA lengths were similar to those for wild type. This is the expected result if the RNAi causes accumulation of intact (polyadenylated) mRNAs. Depletion of XRNA did not affect the profile either for all genes (Fig. 2) or for those mRNAs whose degradation was clearly delayed by XRNA depletion (data not shown). This strongly suggests that trypanosome XRNA is a processive enzyme. In contrast, RNAi targeting RRP45, which results in impaired exosome activity, caused a change in the profile that suggested an accumulation of degradation intermediates containing the 5′ ends of mRNAs. This could only happen if mRNAs had been deadenylated, then subjected to the action of limiting amounts of a distributive 3′–5′ exoribonuclease. We do not know why these mRNAs were not then degraded by XRNA instead; interactions between the exosome and the decapping complex or XRNA cannot be ruled out. The distributive 3′–5′ activity could come either from limiting amounts of the exosome or from a different 3′–5′ exoribonuclease.

Cytoplasmic mRNA that is targeted by Opisthokont exosome is thought to be threaded through a hole in the exosome core, then degraded by the exoribonuclease Rrp44/Dis3, which is situated at the pore exit (Wang et al. 2007; Bonneau et al. 2009). Rrp44 is a processive enzyme (Lorentzen and Conti 2005; Liu et al. 2006; Dziembowski et al. 2007). So far, however, there is no evidence for an association between the trypanosome exosome and the trypanosome Rrp44 homolog (Estévez et al. 2001, 2003). Instead, trypanosome exosomes contain a homolog of Rrp6 (Estévez et al. 2001, 2003; Haile et al. 2007). In yeast and mammals, Rrp6 is associated predominantly with nuclear exosomes and, interestingly, it is a distributive enzyme (e.g., Liu et al. 2007; Januszyk et al. 2011). Evidence from cryo-electron microscopy and X-ray crystallography also so far suggests that RRP6 is located on one side of the exosome, rather than at the pore exit (Cristodero et al. 2008; Makino et al. 2013). It is therefore possible that, in trypanosomes, exosomal degradation of mRNAs is indeed distributive.

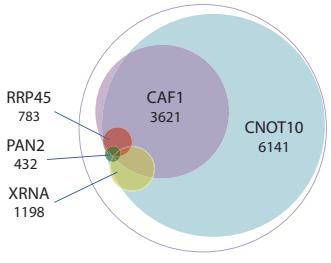

FIGURE 7. Some mRNAs are stabilized in all RNAi lines. The ORFs with at least twofold increased half-lives were selected for each RNAi line. The Venn diagram shows the overlaps between the different lines. The complete gene set is represented by the largest circle.

Our previous studies of 3′–5′ mRNA decay in bloodstream-form trypanosomes focused on very few transcripts (Haile et al. 2003; Schwede et al. 2008, 2009; Färber et al. 2013). The data described here show that results from individual mRNAs cannot be generalized in order to make conclusions about all mRNAs with a particular half-life. Our results are, however, consistent with previous evidence that the 5′–3′ and 3′–5′ pathways can operate independently on a relatively unstable mRNA (Irmer and Clayton 2001; Haile et al. 2003; Li et al. 2006; Schwede et al. 2009). We already saw that many of these are stabilized after XRNA depletion (Manful et al. 2011). Our current finding that CAF1 and CNOT10 depletion had less effect on degradation of the least unstable mRNAs than on those with intermediate stability (Fig. 4B) also fits the model. Most of the mRNAs that showed at least twofold increases in half-life after XRNA depletion (Manful et al. 2011) were affected by CAF1 or CNOT10 depletion but there was very little overlap between these and those that were stabilized after loss of RRP45 or PAN2 (Fig. 7). All mRNAs that were stabilized after PAN2 depletion, and the majority of those that were stabilized after RRP45 depletion, were also dependent on the CAF1/NOT complex and there was a little under 50% overlap between these two gene sets (Fig. 7). This makes sense for the exosome, which can only act after poly(A)-binding protein has been removed from the 3′ end; and it is consistent with other data suggesting that PAN2 alone does not normally effect complete deadenylation (Chen and Shyu 2011).

MATERIALS AND METHODS

Cell lines and culture

Trypanosoma brucei bloodstream forms expressing the *tet* repressor were cultivated as described previously (Alibu et al. 2004). Cell lines used had tetracycline-inducible RNAi targeting *CAF1* (Schwede et al. 2008), *CNOT10* (Färber et al. 2013), PAN2 (Schwede et al. 2009), or RRP45 (Estévez et al. 2001). Cells were grown without selecting antibiotics for 24 h, then RNAi was induced by addition of 100 ng/mL tetracycline for 24 h. Tetracycline treatment alone does not affect the transcriptome (Manful et al. 2011). For analysis of RNA degradation, cells were treated with Sinefungin (final concentration 2 µg/mL) for 5 min, then Actinomycin D was added (final concentration 10 µg/mL) and cells were incubated for a further 30 min for the RNA-seq analysis, or for additional times for the time courses. The time taken to centrifuge the cells (at room temperature) was included as part of the incubation time.

RNA analysis

Total RNA was extracted using peqGold Trifast (peqLab). For quality control RNA was run on a formaldehyde gel and blotted onto Nytran membranes (GE Healthcare). Northern blots were hybridized with radioactively labeled probes for open reading frames (ORFs) (Prime-IT RmT Random Primer Labeling Kit, Stratagene) or with a 5′-phosphorylated *SL* oligonucleotide CZ4490 CAATATAGTA CAGAAACTGTTCTAATAATAGCGTTAGTT. Signals were measured using a phosphorimager. Either the signal of the signal recognition particle (7SL) or the rRNA bands were used for normalization, with similar results.

For high-throughput sequencing, rRNA was depleted using the RiboMinus Eukaryote Kit for RNA-seq (Invitrogen). After RNA fragmentation, libraries were constructed and sequenced at the Heidelberg University Bioquant sequencing facility using Illumina kits.

Bioinformatics

The analyses were done as described previously (Manful et al. 2011). Seventy-six-nucleotide reads were aligned to the *T. brucei* TREU 927 genome, supplemented by all available VSG ORFs from *T. brucei* Lister 427 (Hertz-Fowler et al. 2008) using Bowtie (Langmead et al. 2009) and allowing two mismatches. Read counts for each chosen region were calculated using SAMtools (Li et al. 2009). To avoid counting multicopy sequences more than once, we then took a nonredundant gene list (Siegel et al. 2010) supplemented by a few additional unique genes before calculating the read counts per million reads (RPM) and normalizing. Data were normalized from the average mRNA *SL* signal on Northern blots, except in the case of the *RRP45* RNAi, for which the α tubulin mRNA level was used (for explanation, see Results). Half-lives were calculated assuming exponential decay, using the formula:

$$t1/2 = \ln(2) \times 30/ - \ln(\text{"fraction of RPM left at 30 min"}).$$

In the Tables, the maximum half-life is set to 240 min because of the limitations of using single time point. Supplemental Table S2 (half-lives) contains all annotated genes (coding and noncoding) with the exception of rRNAs. In order to analyze the read densities across mRNAs, we assigned predominant splice and poly(A) sites using all our available data (Manful et al. 2011; Droll et al. 2013). Custom PERL and R scripts were written as required.

Supplemental Table S3 (Differential expression) includes all known genes minus rRNAs. Transcripts of genes <250 bp in length (the maximum insert size selected during RNA-seq library preparations) were not expected to be sequenced, but their precursors might have been. Since the precise size cutoff is bound to vary between replicates, we needed to control for random inclusion of transcripts in this size range. Genes of <250 bp with a relative standard deviation (standard deviation/mean) between replicates at a steady state of >0.3 in either wild-type or knockdown cell lines were therefore excluded from the tables. Differential expression was analyzed using DESeq (Anders and Huber 2010), with a cutoff *P*-adjusted-value <0.01.

Class enrichment

Genes were classified into 72 functional classes, based on annotations and publications, with 4691 (40%) genes remaining unclassified (Supplemental Tables S2, S3). Within a list of genes, class enrichment was estimated using a PERL module for the right-handed Fisher exact test (Banerjee and Pedersen 2003). The unique coding gene list was used for this calculation. Class enrichment heat maps were plotted in R using log10 of *P*-values.

SUPPLEMENTAL MATERIAL

Supplemental material is available for this article.

ACKNOWLEDGMENTS

This work was supported by grants CLl112/9-3 and CLl112/17-1 from the Deutsche Forschungsgemeinschaft (V.F. and D.D.), by the Bundesministerium für Bildung und Forschung, Sysmo project "The Silicon Trypanosome" (A.F. and Janine Philipp), and by a bridging project grant from the ZMBH-DKFZ alliance (V.F.). We thank Janine Philipp, Ute Leibfried, and Claudia Hartman for technical assistance, and David Ibberson (Bioquant sequencing facility) for library production and useful advice.

Received January 21, 2013; accepted March 28, 2013.

REFERENCES

Acestor N, Panigrahi A, Ogata Y, Anupama A, Stuart K. 2009. Protein composition of *Trypanosoma brucei* mitochondrial membranes. *Proteomics* **9:** 5497–5508.

Alibu VP, Storm L, Haile S, Clayton C, Horn D. 2004. A doubly inducible system for RNA interference and rapid RNAi plasmid construction in *Trypanosoma brucei*. *Mol Biochem Parasitol* **139:** 75–82.

Anders S, Huber W. 2010. Differential expression analysis for sequence count data. *Genome Biol* **11:** R106.

Banerjee S, Pedersen T. 2003. The design, implementation and use of the Ngram statistic package. In Proceedings of the fourth international conference on intelligent text processing and comparative linguistics, 370–381, Mexico City.

Banerjee H, Palenchar J, Lukaszewicz M, Bojarska E, Stepinski J, Jemielity J, Guranowski A, Ng S, Wah D, Darzynkiewicz E, et al. 2009. Identification of the HIT-45 protein from *Trypanosoma brucei* as an FHIT protein/dinucleoside triphosphatase: Substrate specificity studies on the recombinant and endogenous proteins. *RNA* **15:** 1554–1564.

Bonneau F, Basquin J, Ebert J, Lorentzen E, Conti E. 2009. The yeast exosome functions as a macromolecular cage to channel RNA substrates for degradation. *Cell* **139:** 547–559.

Bringaud F, Riviere L, Coustou V. 2006. Energy metabolism of trypanosomatids: Adaptation to available carbon sources. *Mol Biochem Parasitol* **149:** 1–9.

Chekanova JA, Gregory BD, Reverdatto SV, Chen H, Kumar R, Hooker T, Yazaki J, Li P, Skiba N, Peng Q, et al. 2007. Genome-wide high-resolution mapping of exosome substrates reveals hidden features in the *Arabidopsis* transcriptome. *Cell* **131:** 1340–1353.

Chen CY, Shyu AB. 2011. Mechanisms of deadenylation-dependent decay. *Wiley Interdiscip Rev RNA* **2:** 167–183.

Colasante C, Ellis M, Ruppert T, Voncken F. 2006. Comparative proteomics of glycosomes from bloodstream form and procyclic culture form *Trypanosoma brucei brucei*. *Proteomics* **6:** 3275–3293.

Colasante C, Robles A, Li C-H, Schwede A, Benz C, Voncken F, Guilbride DL, Clayton C. 2007. Regulated expression of glycosomal phosphoglycerate kinase in *Trypanosoma brucei*. *Mol Biochem Parasitol* **151:** 193–204.

Collart M, Panasenko O. 2012. The Ccr4–Not complex. *Gene* **492:** 42–53.

Cristodero M, Böttcher B, Diepholz M, Scheffzeck K, Clayton C. 2008. The exosome of *Leishmania tarentolae*: Purification and structural analysis by electron microscopy. *Mol Biochem Parasitol* **159:** 24–29.

Daniels J, Gull K, Wickstead B. 2010. Cell biology of the trypanosome genome. *Microbiol Mol Biol Rev* **74:** 552–569.

De Lange T, Michels P, Veerman H, Cornelissen A, Borst P. 1984. Many trypanosome messenger RNAs share a common 5′ terminal sequence. *Nucleic Acids Res* **12:** 3777–3790.

Deneke C, Lipowsky R, Valleriani A. 2013. Complex degradation processes lead to non-exponential decay patterns and age-dependent decay rates of messenger RNA. *PLoS One* **8:** e55442.

Dohm JC, Lottaz C, Borodina T, Himmelbauer H. 2008. Substantial biases in ultra-short read data sets from high-throughput DNA sequencing. *Nucleic Acids Res* **36:** e105.

Doniger T, Katz R, Wachtel C, Michaeli S, Unger R. 2010. A comparative genome-wide study of ncRNAs in trypanosomatids. *BMC Genomics* **11:** 615.

Droll D, Minia I, Fadda A, Singh A, Stewart M, Queiroz R, Clayton C. 2013. Post-transcriptional regulation of the trypanosome heat shock response by a zinc finger protein. *PLoS Pathog* **9:** e1003286.

Dziembowski A, Lorentzen E, Conti E, Séraphin B. 2007. A single subunit, Dis3, is essentially responsible for yeast exosome core activity. *Nat Struct Mol Biol* **14:** 15–22.

Estévez A, Kempf T, Clayton CE. 2001. The exosome of *Trypanosoma brucei*. *EMBO J* **20:** 3831–3839.

Estévez AM, Lehner B, Sanderson CM, Ruppert T, Clayton C. 2003. The roles of inter-subunit interactions in exosome stability. *J Biol Chem* **278:** 34943–34951.

Färber V, Erben E, Sharma S, Stoecklin G, Clayton C. 2013. Trypanosome CNOT10 is essential for the integrity of the NOT deadenylase complex and for degradation of many mRNAs. *Nucleic Acids Res* **41:** 1211–1222.

Fernández-Moya S, Estévez A. 2010. Posttranscriptional control and the role of RNA-binding proteins in gene regulation in trypanosomatid protozoan parasites. *Wiley Interdiscip Rev RNA* **1:** 34–46.

Grigull J, Mnaimneh S, Pootoolal J, Robinson M, Hughes T. 2004. Genome-wide analysis of mRNA stability using transcription inhibitors and microarrays reveals posttranscriptional control of ribosome biogenesis factors. *Mol Cell Biol* **24:** 5534–5547.

Gudipati R, Xu Z, Lebreton A, Séraphin B, Steinmetz L, Jacquier A, Libri D. 2012. Extensive degradation of RNA precursors by the exosome in wild-type cells. *Mol Cell* **48:** 409–421.

Haanstra J, Stewart M, Luu V-D, van Tuijl A, Westerhoff H, Clayton C, Bakker B. 2008. Control and regulation of gene expression: Quantitative analysis of the expression of phosphoglycerate kinase in bloodstream form *Trypanosoma brucei*. *J Biol Chem* **283:** 2495–2507.

Haile S, Estévez AM, Clayton C. 2003. A role for the exosome in the initiation of degradation of unstable mRNAs. *RNA* **9:** 1491–1501.

Haile S, Cristodero M, Clayton C, Estévez A. 2007. The subcellular localisation of trypanosome RRP6 and its association with the exosome. *Mol Biochem Parasitol* **151:** 52–58.

Haile S, Dupe A, Papadopoulou B. 2008. Deadenylation-independent stage-specific mRNA degradation in *Leishmania*. *Nucleic Acids Res* **36:** 1634–1644.

Hertz-Fowler C, Figueiredo LM, Quail MA, Becker M, Jackson A, Bason N, Brooks K, Churcher C, Fahkro S, Goodhead I, et al. 2008. Telomeric expression sites are highly conserved in *Trypanosoma brucei*. *PLOS One* **3:** e3527.

Houalla R, Devaux F, Fatica A, Kufel J, Barrass D, Torchet C, Tollervey D. 2006. Microarray detection of novel nuclear RNA substrates for the exosome. *Yeast* **23:** 439–454.

Irmer H, Clayton CE. 2001. Degradation of the *EP1* mRNA in *Trypanosoma brucei* is initiated by destruction of the 3′-untranslated region. *Nucleic Acids Res* **29:** 4707–4715.

Januszyk K, Liu Q, Lima CD. 2011. Activities of human RRP6 and structure of the human RRP6 catalytic domain. *RNA* **17:** 1566–1577.

Kiss DL, Andrulis ED. 2010. Genome-wide analysis reveals distinct substrate specificities of Rrp6, Dis3, and core exosome subunits. *RNA* **16:** 781–791.

Kolev N, Franklin J, Carmi S, Shi H, Michaeli S, Tschudi C. 2010. The transcriptome of the human pathogen *Trypanosoma brucei* at single-nucleotide resolution. *PLoS Pathog* **6:** e1001090.

Kramer S, Carrington M. 2011. *Trans*-acting proteins regulating mRNA maturation, stability and translation in trypanosomatids. *Trends Parasitol* **27:** 23–30.

Langmead B, Trapnell C, Pop M, Salzberg S. 2009. Ultrafast and memory-efficient alignment of short DNA sequences to the human genome. *Genome Biol* **10:** R25.

Li Y, Kiledjian M. 2010. Regulation of mRNA decapping. *Wiley Interdiscip Rev RNA* **1:** 15.

Li C-H, Irmer H, Gudjonsdottir-Planck D, Freese S, Salm H, Haile S, Estévez AM, Clayton CE. 2006. Roles of a *Trypanosoma brucei*

5′ → 3′ exoribonuclease homologue in mRNA degradation. *RNA* **12:** 2171–2186.
Li H, Handsaker B, Wysoker A, Fennell T, Ruan J, Homer N, Marth G, Abecasis G, Durbin R. 2009. The Sequence Alignment/Map format and SAMtools. *Bioinformatics* **25:** 2078–2079.
Liu Q, Greimann JC, Lima CD. 2006. Reconstitution, activities, and structure of the eukaryotic RNA exosome. *Cell* **127:** 1223–1237.
Liu Q, Greimann JC, Lima CD. 2007. Reconstitution, activities, and structure of the eukaryotic RNA exosome. *Cell* **131:** 188–189.
Lorentzen E, Conti E. 2005. Structural basis of 3′ end RNA recognition and exoribonucleolytic cleavage by an exosome RNase PH core. *Mol Cell* **11:** 473–481.
Makino DL, Baumgartner M, Conti E. 2013. Crystal structure of an RNA-bound 11-subunit eukaryotic exosome complex. *Nature* **495:** 70–75.
Manful T, Fadda A, Clayton C. 2011. The role of the 5′–3′ exoribonuclease XRNA in transcriptome-wide mRNA degradation. *RNA* **17:** 2039–2047.
Mauxion F, Prève B, Séraphin B. 2013. C2ORF29/CNOT11 and CNOT10 form a new module of the CCR4-NOT complex. *RNA Biol* **10:** 1–10.
Michaeli S. 2011. *Trans*-splicing in trypanosomes: Machinery and its impact on the parasite transcriptome. *Future Microbiol* **6:** 459–474.
Michaeli S, Doniger T, Gupta SK, Wurtzel O, Romano M, Visnovezky D, Sorek R, Unger R, Ullu E. 2012. RNA-seq analysis of small RNPs in *Trypanosoma brucei* reveals a rich repertoire of non-coding RNAs. *Nucleic Acids Res* **40:** 1282–1298.
Michels PA, Bringaud F, Herman M, Hannaert V. 2006. Metabolic functions of glycosomes in trypanosomatids. *Biochim Biophys Acta* **1763:** 1463–1477.
Miller C, Schwalb B, Maier K, Schulz D, Dümcke S, Zacher B, Mayer A, Sydow J, Marcinowski L, Dölken L, et al. 2011. Dynamic transcriptome analysis measures rates of mRNA synthesis and decay in yeast. *Mol Syst Biol* **7:** 458.
Milone J, Wilusz J, Bellofatto V. 2004. Characterization of deadenylation in trypanosome extracts and its inhibition by poly(A)-binding protein Pab1p. *RNA* **10:** 448–457.
Mnaimneh S, Davierwala AP, Haynes J, Moffat J, Peng WT, Zhang W, Yang X, Pootoolal J, Chua G, Lopez A, et al. 2004. Exploration of essential gene functions via titratable promoter alleles. *Cell* **118:** 31–44.
Muller M, Padmanabhan PK, Rochette A, Mukherjee D, Smith M, Dumas C, Papadopoulou B. 2010. Rapid decay of unstable *Leishmania* mRNAs bearing a conserved retroposon signature 3′-UTR motif is initiated by a site-specific endonucleolytic cleavage without prior deadenylation. *Nucleic Acids Res* **38:** 5867–5883.
Nilsson D, Gunasekera K, Mani J, Osteras M, Farinelli L, Baerlocher L, Roditi I, Ochsenreiter T. 2010. Spliced leader trapping reveals widespread alternative splicing patterns in the highly dynamic transcriptome of *Trypanosoma brucei*. *PLoS Pathog* **6:** e1001037.
Ouellette M, Papadopoulou B. 2009. Coordinated gene expression by post-transcriptional regulons in African trypanosomes. *J Biol* **8:** 100.
Palenchar JB, Bellofatto V. 2006. Gene transcription in trypanosomes. *Mol Biochem Parasitol* **146:** 135–141.
Panigrahi A, Ogata Y, Zíková A, Anupama A, Dalley R, Acestor N, Myler P, Stuart K. 2008. A comprehensive analysis of *Trypanosoma brucei* mitochondrial proteome. *Proteomics* **9:** 434–450.
Schoenberg DR. 2011. Mechanisms of endonuclease-mediated mRNA decay. *Wiley Interdiscip Rev RNA* **2:** 582–600.
Schwede A, Ellis L, Luther J, Carrington M, Stoecklin G, Clayton C. 2008. A role for Caf1 in mRNA deadenylation and decay in trypanosomes and human cells. *Nucleic Acids Res* **36:** 3374–3388.
Schwede A, Manful T, Jha B, Helbig C, Bercovich N, Stewart M, Clayton C. 2009. The role of deadenylation in the degradation of unstable mRNAs in trypanosomes. *Nucleic Acids Res* **37:** 5511–5528.
Sendler E, Johnson GD, Krawetz SA. 2011. Local and global factors affecting RNA sequencing analysis. *Anal Biochem* **419:** 317–322.
Siegel T, Hekstra D, Wang X, Dewell S, Cross G. 2010. Genome-wide analysis of mRNA abundance in two life-cycle stages of *Trypanosoma brucei* and identification of splicing and polyadenylation sites. *Nucleic Acids Res* **38:** 4946–4957.
Sun M, Schwalb B, Schulz D, Pirkl N, Etzold S, Larivière L, Maier K, Seizl M, Tresch A, Cramer P. 2012. Comparative Dynamic Transcriptome Analysis (cDTA) reveals mutual feedback between mRNA synthesis and degradation. *Genome Res* **22:** 1350–1359.
Ullu E, Tschudi C. 1991. *Trans* splicing in trypanosomes requires methylation of the 5′ end of the spliced leader RNA. *Proc Natl Acad Sci* **88:** 10074–10078.
Utter C, Garcia S, Milone J, Bellofatto V. 2011. Poly(A)-specific Ribonuclease (PARN-1) function in stage-specific mRNA turnover in *Trypanosoma brucei*. *Eukaryot Cell* **10:** 1230–1240.
Vertommena D, Van Roy J, Szikora J-P, Ridera M, Michels P, Opperdoes F. 2008. Differential expression of glycosomal and mitochondrial proteins in the two major life-cycle stages of *Trypanosoma brucei*. *Mol Biochem Parasitol* **158:** 189–201.
Wang H-W, Wang J, Ding F, Callahan K, Bratkowski M, Butler J, Nogales E, Ke A. 2007. Architecture of the yeast Rrp44–exosome complex suggests routes of RNA recruitment for 3′ end processing. *Proc Natl Acad Sci* **104:** 16844–16849.
Wyers F, Rougemaille M, Badis G, Rousselle J, Dufour M, Boulay J, Regnault B, Devaux F, Namane A, Seraphin B, et al. 2005. Cryptic pol II transcripts are degraded by a nuclear quality control pathway involving a new poly(A) polymerase. *Cell* **121:** 725–737.
Yamashita A, Chang TC, Yamashita Y, Zhu W, Zhong Z, Chen CY, Shyu AB. 2005. Concerted action of poly(A) nucleases and decapping enzyme in mammalian mRNA turnover. *Nat Struct Mol Biol* **12:** 1054–1063.
Zheng W, Chung LM, Zhao H. 2011. Bias detection and correction in RNA-Sequencing data. *BMC Bioinformatics* **12:** 290.